Multi-satellite data depicts record-breaking methane leak from a well blowout

Luis Guanter[1,2*], Javier Roger[1], Shubham Sharma[3], Adriana Valverde[1], Itziar Irakulis-Loitxate[4,1], Javier Gorroño[1], Xin Zhang[3], Berend J. Schuit[3,5], Joannes D. Maasakkers[3], Ilse Aben[3], Alexis Groshenry[6], Antoine Benoit[6], Quentin Peyle[6], Daniel Zavala-Araiza[2]

[1]*Research Institute of Water and Environmental Engineering (IIAMA), Universitat Politècnica de València, Spain.*
[2]*Environmental Defense Fund, Amsterdam, Netherlands*
[3]*SRON Netherlands Institute for Space Research, Leiden, Netherlands*
[4]*International Methane Emissions Observatory, United Nations Environment Programme, Paris, France*
[5]*GHGSat Inc., Montreal, Canada*
[6]*Kayrros, Paris, France*

*To whom correspondence should be addressed; E-mail: lguanter@fis.upv.es

Accidental blowouts in oil and gas wells can result in large and prolonged methane emissions, which are often unreported when happening in remote places. The rapid advancement of space-based methods for detecting and quantifying methane plumes provides an essential tool for uncovering these super-emission events. We use a range of methane-sensitive satellites to document a methane leak from a well blowout in Kazakhstan's Karaturun East oil field in 2023. A dense time series of observations from multiple satellites shows that the leak was active during 205 days. Using 48 high-quality plume observations from this time series, we estimate that a total of 128±36 kt of methane were released to the atmosphere during this leak. Our results reveal that the total methane emissions from the Karaturun 2023 event exceeded those from all previously documented accidents, and highlight the pivotal role of satellites in detecting and quantifying large methane plumes around the planet.

Introduction

Human-induced methane emissions are responsible for about 30% of the global warming since the pre-industrial period[1]. The oil and gas industry accounts for a large share of those emissions[2], although the mitigation of oil and gas emissions has actually been found to be technically feasible and cost-effective[3]. This holds particularly true for high-emitting point sources, also known as super-emitters[4]. Methane super-emitters in the oil and gas industry are usually linked to unexpected infrastructure failures, including blowouts during drilling, completion, or production activities in oil and gas wells. Well blowouts result in uncontrolled releases of substantial amounts of natural gas, consisting primarily of methane. However, it is difficult to achieve a global perspective of the methane emissions originated by blowouts in oil and gas wells, as these accidents often occur in remote areas, which complicates the acquisition of surface and airborne measurements.

A growing constellation of methane-sensitive satellites is now improving our ability to detect and monitor large methane leaks around the planet. This constellation comprises the Sentinel-5P/TROPOMI mission and a number of high spatial resolution missions, which can be separated in hyperspectral and multispectral missions. TROPOMI provides a systematic daily global surveillance of the largest methane emissions since 2018[5;6]. In contrast, the hyperspectral high-resolution missions have a sparse spatio-temporal sampling as compared with TROPOMI, but scan the Earth at a much higher spatial resolution, which enables the detection of smaller plumes and the attribution of those to facility-level sources. Among these hyperspectral high-resolution missions we find the GHGSat private constellation[7;8], specifically designed for methane and carbon dioxide mapping at 25–50 m resolution, and the EnMAP, PRISMA and EMIT scientific missions, which also have a relatively high sensitivity to methane[9–11]. Finally, the Sentinel-2 and Landsat multispectral radiometers offer a lower sensitivity to methane than the hyperspectral missions, but have a 20-30 spatial sampling and a systematic global coverage every few days[12–14], which compensates for the sporadic and under-demand sampling of the hyperspectral satellites.

There are examples of the potential of the previous satellites to document methane emissions from well blowouts in the last years, although only a few satellite observations were available for each of those studies: Thompson et al. conducted the first detection of an individual methane plume with observations of the 2015 Aliso Canyon event (Los Angeles, USA) by the Hyperion high-resolution spectroscopy demonstration mission[15]; Pandey et al. used one TROPOMI overpass to estimate the emissions caused by a shale gas well blowout in Ohio (USA)[16]; Maasakkers et al. used six TROPOMI overpasses and gas flaring data from the VIIRS satellite instrument to estimate emissions from a natural gas well blowout in Louisiana (USA)[17]; Cusworth et al. combined observations from TROPOMI, GHGSat and PRISMA (four observations in total) to characterise the emissions from a 20-day leak event due to a gas well blowout in the Eagle Ford Shale (USA)[18].

All of those blowouts happened at US sites accessible to well operators and mitigation teams, so the associated emissions could therefore be well documented despite the limited availability of satellite observations. This is not the case of the well blowout at the Karaturun East oil field in Kazakhstan's Mangistau region that we report in this study (Fig. 1), which happened at a remote site. According to media reports, the blowout and subsequent fire happened on the morning of 9 June 2023 during exploration works at well 303[19] (Fig. 1a). The fire destroyed different pieces of safety equipment, leading to a loss of well control and a 10-m high fire blaze. Days later, a 15-m wide crater was formed by the collapse of rocks around the wellhead, which prevented an early seal of the well. The first attempt to halt the flow of gas consisted of pumping thousands of tons of water through two injection holes between 13 October and 20 November. This action mitigated the gas leak, but did not completely resolve it. The flow of gas and the fire could finally be stopped on 25 December 2023 by injecting heavy drilling mud via a special-purpose probe, which connected with the wellbore of the accident well at a depth of about 1000 m[20].

[Figure 1 about here.]

In this work, we use satellites to document the methane emissions originated by the blowout in the Karaturun East oil field. We have generated a dense time series with more than hundred satellite observations from TROPOMI and high-resolution satellites to monitor and quantify the massive methane plumes following this blowout. The satellite data were processed with state-of-the-art algorithms for the detection and quantification of methane plumes from space, optimised for the particular emission intensity and site characteristics of this event (Methods).

Results and discussion

The leak was first detected in global methane concentration data from the Sentinel-5P/TROPOMI mission[19] (Fig. 1b, Fig. S1). The exact location and date of the blowout could be confirmed retrospectively with data from the Sentinel-2 multispectral radiometer, which flew over the site hours after the accident. The evolution of the leak was then monitored with TROPOMI and a range of high-resolution missions (including PRISMA, EnMAP, EMIT, GHGSat and the Sentinel-2 and Landsat-8/9 multispectral radiometers), some of which were specifically tasked to acquire data over the site. Extremely large methane plumes were detected during the entire time series (Fig. 2).

[Figure 2 about here.]

In particular, we detected methane plumes from the site 115 times between 9 June and 25 December 2023. After quality screening of all the detected plumes, we retained 48 for the quantification of emission rates (Methods). We obtained flux rates between 3.6±1.3 and 63±42 t/h, with typical values between 20 and 50 t/h (Fig. 3a, Supplementary Fig. S2, and Supplementary Tables S1 and S2). The most substantial emission rates occurred in the weeks following the blowout (Fig. 3a). Plume intensity gradually decreased over time until the leak repair on 25 December. Notably, a relatively large plume of 12±3 t/h was detected by GHGSat on 25 December, which suggests that the satellite flew over the site shortly before the final repair action on the same day. Three subsequent observations on 1, 12 and 14 January 2024 confirmed the definitive cessation of the leak.

[Figure 3 about here.]

We utilized a time series of fire radiative power derived from the VIIRS FIRMS satellite product to track the fire intensity during the event (Methods). Additionally, we used observations from high resolution satellites to detect (albeit not quantify) fire at the site. We found that the strongest fire occurred immediately after the well blowout, and kept a relatively high intensity during about 20 days (Fig. 3b). Subsequently, the fire remained active as indicated by the fire detections from the high resolution satellites, but its intensity decreased. The fire intensity in this event is actually substantially lower than that of strong flares in oil and gas installations, and also than the intensity of the fires measured during the Louisiana 2019 blowout event[17] (Supplementary Fig. S3). The relatively low intensity of the fire at the Karaturun East site would indicate that only a small fraction of the gas outflow was flared. It is unclear whether the accident well 303 was an oil or a gas well, but in the first case it could be hypothesized that the 2-phase oil and gas mixture led to a low combustion efficiency during the event[21].

To give context to the magnitude of the methane plumes detected during the entire Karaturun East leak, the majority of plumes identified in this event exceeded 10 t/h and are comparable to the largest individual plumes detected using global TROPOMI data worldwide[5;6]. We obtain an estimate of 128±36 kt for the total amount of methane released to the atmosphere during the event (Methods). This is substantially larger than the total emission of 97 kt (no uncertainty available) reported for the outstanding 2015 Aliso Canyon blowout[22], which is considered the largest methane leak from regular oil and gas operations documented to date. The total emission from the Karaturun event also exceeds the estimates for the massive releases from the Ohio 2018[16] and the Louisiana 2019[17] blowout events, for which 60±15 kt and 21–63 kt (95% confidence interval) were estimated, respectively (Fig. 3c). Only the sabotage of the Nord Stream 1 and 2 subsea twin pipelines in the Baltic Sea on 26 September 2022, for which a total of 420-490 kt (95% confidence interval) has been estimated[23], may have led to greater emissions than the Karaturun 2023 blowout event.

Our results show that the 2023 well blowout in Kazakhstan's Karaturun East oil field has likely caused the largest methane emission from an infrastructure accident ever documented. The detection and quantification of this leak has only been possible because of the recent availability of methane-sensitive satellites. It is unknown how many of such large methane leaks from oil and gas infrastructure failures may have occurred in the last decades around the world, and how this may have led to underestimated emission inventories. The new era of methane monitoring from space, boosted by international initiatives such as the Methane Alert and Response System (MARS)[24] of the United Nations Environment Programme, and new methane satellite missions such as MethaneSAT[25] and Carbon Mapper[26], will be crucial for the detection and quantification of large methane leaks around the world.

Methods

Satellite data

We generated a dense time series of methane observations over the Karaturun East site using TROPOMI and high-resolution satellite missions. The latter included hyperspectral observations from the GHGSat private satellite constellation, which offers the highest sensitivity to methane for this type of high-emitting point source, as well as from the public hyperspectral missions EnMAP (German Aerospace Agency, Germany), PRISMA (Italian Space Agency, Italy) and EMIT (NASA Jet Propulsion Laboratory, USA), which share a relatively similar configuration, a medium-high sensitivity to methane, and an open data policy. Acquisitions from the less sensitive Sentinel-2 and Landsat multispectral radiometers were mostly used for plume detection along the entire time period. A total of 115 plumes were detected between 9 June and 25 December 2023 (26 from TROPOMI and 89 from the high resolution satellites). After quality control, 48 of those plumes (15 from TROPOMI and 33 from the high resolution satellites) were retained for the quantification of emissions (Supplementary Figure S2).

Satellite data were also used to monitor fire activity at the site. Fire radiative power data from the Fire Information for Resource Management System (FIRMS) based on VIIRS data were used to assess the evolution of fire intensity (Fig. 3b and Supplementary Fig. S3). In addition, the observations from the high resolution satellites from which we derived methane plumes were also utilised to detect (but not quantify) smaller active fires at the site.

Quantification of methane plumes with high spatial resolution satellites

For the retrieval of methane plume information from EnMAP, PRISMA and EMIT hyperspectral data, we optimised the widely-used matched-filter approach to deal with the large plumes and high methane concentration values found during the Karaturun East leak. This included the implementation of a log-normal version of the matched filter and the removal of plume pixels when calculating the statistics needed for the matched-filter, as described in Pei et al.[27]. The $\triangle XCH_4$ maps obtained with this retrieval were screened for quality (cloud-free observations, no retrieval artifacts, no substantial fractions of the plume lying outside the image area).

The selected high-quality observations were used for the subsequent flux rate estimation. We manually delineated the plumes and calculated the integrated methane enhancement (IME), which is the total mass of methane contained in the plume. The IME values were converted into flux rate estimates using the IME-based model[28], which relates the IME, the plume length, and an effective wind speed parameter (U_{eff}) to the flux rate. For U_{eff}, we used emipirical linear models linking U_{eff} with 10-m wind speed data (U_{10}). These models were specifically derived for the typical ΔXCH_4 retrieval precision and plume length estimated for this event (simulated plumes are 5-10 km long). One common $U_{\text{eff}} - U_{10}$ model was used for EnMAP and PRISMA, which share the same 30-m resolution and retrieval precision, and a second one was derived for EMIT in order to account for its 60 m pixels (Supplementary Fig. S4). Uncertainties in flux rate estimates were derived assuming a 50% uncertainty in the input wind speed data, which is consistent with previous studies.

In the case of the multispectral missions (Sentinel-2 and Landsat), we have followed the approach described in Gorroño et al.[13]. Same as for the hyperspectal data, this approach consists of a two-step processing scheme, in which ΔXCH_4 maps are first derived with a multi-band and multi-pass retrieval, and the flux rates are subsequently estimated using the IME-based method. Since the methane sensitivity of the multispectral missions is lower than that of GHGSat and the hyperspectral missions, data from Sentinel-2 and Landsat were mostly used to detect methane plumes during the event. Thanks to their systematic acquisitions and combined revisit time of 2-3 days, more than 70 methane plumes could be detected with Sentinel-2 and Landsat. In addition, 5 of them acquired under optimal observation conditions were included in the list of 48 plumes used for quantification.

Finally, in the case of GHGSat, the physically-based methane concentration retrieval described in Jervis et al.[8] was applied. The performance of GHGSat for the detection and quantification of methane emissions from oil and gas infrastructure has been extensively tested during operations in the last years[7].

Verification of the detection and quantification of methane plumes with high spatial resolution satellites

Our processing chain to convert spectral radiance data cubes to flux rates, which involves ΔXCH_4 retrieval, plume segmentation, and IME-based flux rate estimation, has been validated with controlled methane release tests for all the previous high-resolution instruments[29].

However, since those controlled-release tests were made for plumes weaker than the ones detected in this event, we also used end-to-end simulations to test our ability to quantify flux rates for the large plumes and particular conditions of the Karaturun East site. Real top-of-atmosphere radiance data acquired during the event were used as input for the simulations, so the particular acquisition conditions at the site (atmospheric state, illumination angles, potential water vapour and smoke co-emissions ...) were properly represented. This end-to-end simulation approach has already been applied to hyperspectral and multispectral data[9;13]. In this study, we did the simulations for PRISMA observations of methane plumes over the Karaturun East site within a 5–50 t/h emission range. The results show that our processing is able to produce reliable flux estimates for that entire flux rate range (Supplementary Fig. S5). Even if this end-to-end verification exercise was only done for PRISMA, the overall conclusions can be extended to the other high resolution missions, as they share a relatively similar processing chain.

Those simulations confirm the robustness of our methane retrieval and quantification methods for the particular conditions of the Karaturun East event. In addition, it must be remarked that we do not find any distortion of our ΔXCH_4 maps with the water vapour and smoke being potentially co-emitted by the source (Supplementary Fig. S6). We verified this by generating water vapour anomaly maps using a similar retrieval method as the one we use for methane. The resulting water vapour maps show the expected turbulence patterns, but no water vapour plume superposed to the methane plumes. Also, we do not detect any smoke signal in the 2300 nm spectral window used for the methane retrievals, indicating that the smoke plumes may not have a relevant optical activity in this spectral range for this event, which has also been found in previous studies[10].

Quantification of methane plumes with TROPOMI

TROPOMI (aboard Sentinel-5P)[30] observes methane with high precision at a resolution of $5.5\times7\,\text{km}^2$, allowing detection of the plume further downwind. We used the Weather Research and Forecast (WRF) version 4.1[31] to simulate the enhanced methane concentrations associated with the blowout at a resolution of $3\times3\,\text{km}^2$ from June to December 2023. We then compared these modelled concentrations to TROPOMI data in a Bayesian inversion framework[32] to infer daily emissions rates. To obtain simulated plumes that best match TROPOMI, we ran WRF using two meteorological boundary conditions products and four planetary boundary layer physics schemes, and sampled the model at several timesteps around the TROPOMI overpass. Based on daily inversions with all model setups, we selected the simulations that gave the lowest posterior observation cost for each day to be used. We only report quantifications for days with clear plumes and good matches with simulated plumes based on visual inspection. To estimate uncertainty, we built an ensemble of inversions by varying critical inversion parameters such as data filtering and the selected simulation. We conservatively report the 2-standard deviation range from the ensemble as uncertainty. Details on the TROPOMI quantification approach are given in the Supplementary Text S1.

Quantification of total methane emission

We estimate a total of 128±36 kt of methane being released to the atmosphere between 9 June and 25 December. This amount was calculated through the integration of a polynomial fitted to the time series of 48 flux rate estimates from the plume data passing the quality screening (Fig. 3a). The estimation of the uncertainty associated to the total emission is the result of propagating the uncertainty from each flux rate estimate through the flux rate interpolation and curve integration using multivariate Monte Carlo simulations. We assume a 50% correlation between flux rate errors in order to account for both uncorrelated error components (e.g. plume shape changes) and correlated error components (e.g. same source area) (Supplementary Fig. S7).

We tested an alternative option for the quantification of the total emission. This consisted in using only the most accurate flux rate estimates from GHGSat and the hyperspectral missions, which are a priori the best suited satellites for the quantification of single plumes over a relatively complex surface. This alternative approach prioritises the quality of observations over quantity. For this alternative approach, we found similar total emission numbers than for the default all-satellite configuration, but the uncertainty of the total emission was substantially lower for the latter case with all 48 plumes (36 versus 58 t/h, Supplementary Fig. S7), so we opted for using all the available high-quality observations for the calculation of the total emission and its uncertainty.

List of Supplementary Materials

- Text S1
- Tables S1 and S2
- Figures S1–S7

References

1. Dhakal, S. *et al.* Emissions trends and drivers. In Shukla, P. *et al.* (eds.) *Climate Change 2022: Mitigation of Climate Change. Contribution of Working Group III to the Sixth Assessment Report of the Intergovernmental Panel on Climate Change*, book section 2 (Cambridge University Press, Cambridge, UK and New York, NY, USA).

2. Saunois, M. *et al.* The global methane budget 2000–2017. *Earth System Science Data* **12**, 1561–1623 (2020).

3. Ocko, I. *et al.* Acting rapidly to deploy readily available methane mitigation measures by sector can immediately slow global warming. *Environmental Research Letters* **16** (2021).

4. Zavala-Araiza, D. *et al.* Reconciling divergent estimates of oil and gas methane emissions **112**, 15597–15602 (2015).

5. Lauvaux, T. *et al.* Global assessment of oil and gas methane ultra-emitters. *Science* **375**, 557–561 (2022).

6. Schuit, B. J. *et al.* Automated detection and monitoring of methane super-emitters using satellite data. *Atmospheric Chemistry and Physics* **23**, 9071–9098 (2023).

7. Varon, D. J. *et al.* Satellite Discovery of Anomalously Large Methane Point Sources From Oil/Gas Production. *Geophysical Research Letters* **46**, 13507–13516.

8. Jervis, D. *et al.* The GHGSat-D imaging spectrometer. *Atmospheric Measurement Techniques* **14**, 2127–2140 (2021).

9. Guanter, L. *et al.* Mapping methane point emissions with the PRISMA spaceborne imaging spectrometer. *Remote Sensing of Environment* **265**, 112671 (2021).

10. Roger, J. *et al.* High-resolution methane mapping with the EnMAP satellite imaging spectroscopy mission. *IEEE Transactions on Geoscience and Remote Sensing* 1–1 (2024).

11. Thorpe, A. K. *et al.* Attribution of individual methane and carbon dioxide emission sources using EMIT observations from space. *Science Advances* **9**, eadh2391 (2023).

12. Varon, D. J. *et al.* High-frequency monitoring of anomalous methane point sources with multispectral sentinel-2 satellite observations. *Atmospheric Measurement Techniques* **14**, 2771–2785 (2021).

13. Gorroño, J., Varon, D. J., Irakulis-Loitxate, I. & Guanter, L. Understanding the potential of Sentinel-2 for monitoring methane point emissions. *Atmospheric Measurement Techniques* **16**, 89–107 (2023).

14. Irakulis-Loitxate, I., Guanter, L., Maasakkers, J. D., Zavala-Araiza, D. & Aben, I. Satellites detect abatable super-emissions in one of the world's largest methane hotspot regions. *Environmental Science & Technology* **56**, 2143–2152 (2022). PMID: 35102741.

15. Thompson, D. R. *et al.* Space-based remote imaging spectroscopy of the Aliso Canyon CH4 superemitter. *Geophysical Research Letters* **43**, 6571–6578 (2016).

16. Pandey, S. *et al.* Satellite observations reveal extreme methane leakage from a natural gas well blowout **116**, 26376–26381 (2019).

17. Maasakkers, J. D. *et al.* Reconstructing and quantifying methane emissions from the full duration of a 38-day natural gas well blowout using space-based observations. *Remote Sensing of Environment* **270**, 112755 (2022).

18. Cusworth, D. H. *et al.* Multisatellite imaging of a gas well blowout enables quantification of total methane emissions. *Geophysical Research Letters* **48**, e2020GL090864.

19. Clark, A. & Gizitdinov, N. Scientists Say They've Detected a Huge Methane Leak in Kazakhstan. *Bloomberg* (2023-08-04).

20. Afanasiev, V. Kazakh operator halts gas fire at well that has been burning since June. *Upstream* (2023-12-27).

21. Understanding wellhead ignition as a blowout response. *Fuel* **243**, 622–629 (2019).

22. Conley, S. *et al.* Methane emissions from the 2015 Aliso Canyon blowout in Los Angeles, CA. *Science* **351**, 1317–1320 (2016).

23. S. Harris et al. Renewed understanding of atmospheric methane emissions from the 2022 Nord Stream pipeline sabotage (2023). Submitted.

24. UNEP-IMEO. Methane Alert and Response System (MARS). `https://www.unep.org/explore-topics/energy/what-we-do/methane/imeo-action/methane-alert-and-response-system-mars` (2023). [Online; accessed 1-February-2024].

25. MethaneSAT. `https://www.methanesat.org/` (2024). [Online; accessed 1-February-2024].

26. Carbon Mapper. `https://carbonmapper.org/` (2024). [Online; accessed 1-February-2024].

27. Pei, Z. *et al.* Improving quantification of methane point source emissions from imaging spectroscopy. *Remote Sensing of Environment* **295**, 113652 (2023).

28. Varon, D. J. *et al.* Quantifying methane point sources from fine-scale satellite observations of atmospheric methane plumes. *Atmospheric Measurement Techniques* **11**, 5673–5686 (2018).

29. Sherwin, E. D. *et al.* Single-blind validation of space-based point-source detection and quantification of onshore methane emissions. *Scientific Reports* **13**, 3836 (2023).

30. Lorente, A., Borsdorff, T., Martinez-Velarte, M. C. & Landgraf, J. Accounting for surface reflectance spectral features in tropomi methane retrievals. *Atmospheric Measurement Techniques* **16**, 1597–1608 (2023).

31. Powers, J. *et al.* The weather research and forecasting (wrf) model: Overview, system efforts, and future directions. *Bulletin of the American Meteorological Society* **98** (2017).

32. Jacob, D. J. *et al.* Quantifying methane emissions from the global scale down to point sources using satellite observations of atmospheric methane. *Atmospheric Chemistry and Physics* **22**, 9617–9646 (2022).

Acknowledgments

This research was funded by the European Space Agency through the HiResCH4 project (contract N.4000134929) and the IMEO Science Studies programme (contracts DTIE22-EN5036 and DTIE23-EN6386). X.Z. acknowledges funding from the Global Methane Hub. We are thankful to Jason McKeever and the GHGSat team for the acquisition and processing of the GHGSat data used in this study. Patrizia Sacco and Ettore Lopinto (Italian Space Agency, ASI) are thanked for the PRISMA acquisitions, and Nicole Pinnel (German Aerospace Center, DLR) and Sabine Chabrillat (GFZ German Research Centre for Geosciences) for the EnMAP acquisitions. We are grateful to Daniel J. Varon for the WRF-LES modelled plumes used in this study. Part of this work was carried out on the Dutch national e-infrastructure, and we thank SURF (www.surf.nl) for the support in using the National Supercomputer Snellius. Correspondence and request for materials should be addressed to L.G.

Author contributions

Conceptualization and methodology: L.G., J.D.M., and I.I.-L. Formal analysis: L.G., J.R., S.S., A.V., I.I.-L., J.G., X. Z., B.J.S., J.D.M., A.G. Investigation: All authors. Supervision: L.G., J.D.M., I.A., Q.P., A.B., D.Z. Writing-original draft: L.G. Writing-review and editing: All authors

Competing interests

The authors declare no competing interests.

List of Figures

1 Blowout and first methane plumes from the 2023 Karaturun East leak. **a**, Location of the well No. 303 (45.3324°N, 52.3730°E) in the Karaturun East oil field where the blowout happened on 9 June 2023, including a view of the active fire at the site (photo from Mangistau Regional Administration). **b**, Synoptic map of total methane concentration (in parts-per-billion, ppb) from a Sentinel-5P/TROPOMI overpass 17 days after the blowout. A large methane plume emitted from the accident well is observable. 13

2 Sample of methane plumes detected with the PRISMA, EMIT, EnMAP and GHGSat satellite sensors on different days. The color scale in the maps represent methane concentration enhancements above background methane levels ($\triangle XCH_4$), expressed in parts-per-billion (ppb). The emission rate (Q) estimated for each plume is provided on the top right side of each map panel. 14

3 Quantification of methane emissions and fire intensity from the Karaturun East 2023 blowout. **a**, Time series of methane emission rates (in metric tonnes per hour, t/h) derived from the satellite observations which passed the quality screening (see also Supplementary Fig. S2). The black line and the shaded area represent the polynomial fit that has been integrated for the calculation of the total amount of methane released during the event. The black bars depict all satellite observations from which a plume could be detected, including those that could not be quantified. **b**, Time series of fire radiative power derived from the VIIRS FIRMS data product. The black bars depict all satellite detections of active fire at the site. **c**, Comparison of the total amount of methane released during the Karaturun East 2023 event with the Aliso Canyon 2015[22], Ohio 2018[16], and Louisiana 2019[17] blowout events also leading to massive methane emissions. 15

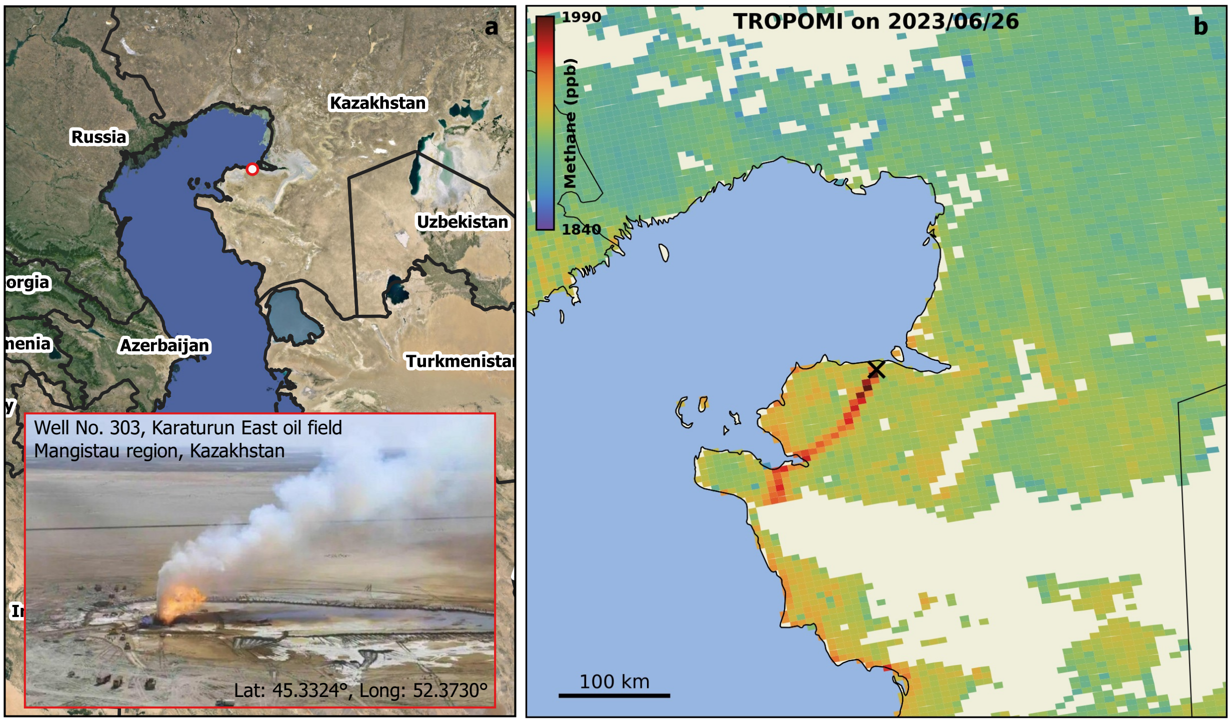

Figure 1: Blowout and first methane plumes from the 2023 Karaturun East leak. **a**, Location of the well No. 303 (45.3324°N, 52.3730°E) in the Karaturun East oil field where the blowout happened on 9 June 2023, including a view of the active fire at the site (photo from Mangistau Regional Administration). **b**, Synoptic map of total methane concentration (in parts-per-billion, ppb) from a Sentinel-5P/TROPOMI overpass 17 days after the blowout. A large methane plume emitted from the accident well is observable.

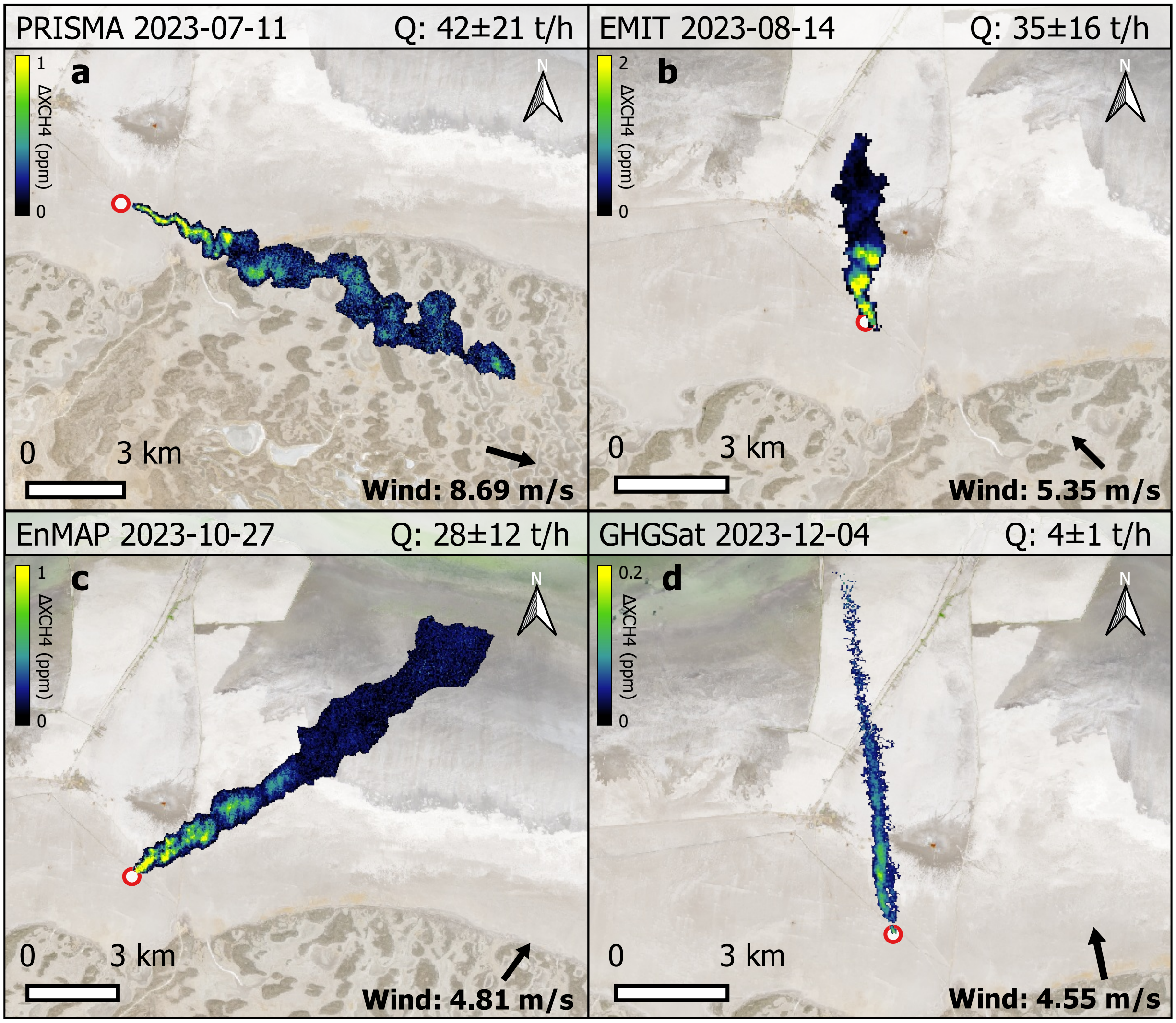

Figure 2: Sample of methane plumes detected with the PRISMA, EMIT, EnMAP and GHGSat satellite sensors on different days. The color scale in the maps represent methane concentration enhancements above background methane levels (ΔXCH_4), expressed in parts-per-billion (ppb). The emission rate (Q) estimated for each plume is provided on the top right side of each map panel.

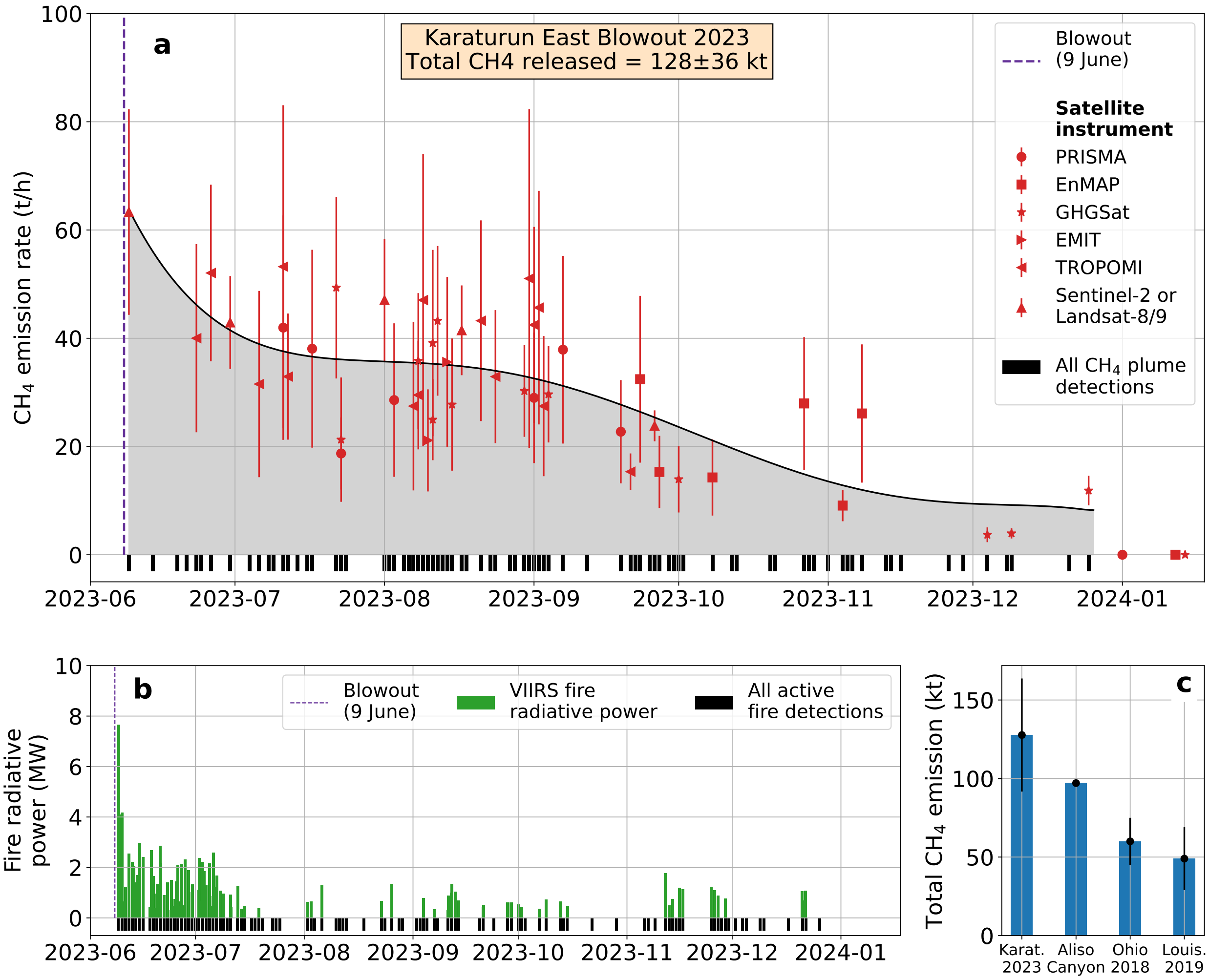

Figure 3: Quantification of methane emissions and fire intensity from the Karaturun East 2023 blowout. **a**, Time series of methane emission rates (in metric tonnes per hour, t/h) derived from the satellite observations which passed the quality screening (see also Supplementary Fig. S2). The black line and the shaded area represent the polynomial fit that has been integrated for the calculation of the total amount of methane released during the event. The black bars depict all satellite observations from which a plume could be detected, including those that could not be quantified. **b**, Time series of fire radiative power derived from the VIIRS FIRMS data product. The black bars depict all satellite detections of active fire at the site. **c**, Comparison of the total amount of methane released during the Karaturun East 2023 event with the Aliso Canyon 2015[22], Ohio 2018[16], and Louisiana 2019[17] blowout events also leading to massive methane emissions.

Supplementary Materials

Multi-satellite data depicts record-breaking methane leak from a well blowout

Luis Guanter[1,2*], Javier Roger[1], Shubham Sharma[3], Adriana Valverde[1], Itziar Irakulis-Loitxate[4,1], Javier Gorroño[1], Xin Zhang[3], Berend J. Schuit[3,5], Joannes D. Maasakkers[3], Ilse Aben[3], Alexis Groshenry[6], Antoine Benoit[6], Quentin Peyle[6], Daniel Zavala-Araiza[2]

[1]Research Institute of Water and Environmental Engineering (IIAMA), Universitat Politècnica de València, Spain.

[2]Environmental Defense Fund, Amsterdam, Netherlands

[3]SRON Netherlands Institute for Space Research, Leiden, Netherlands

[4]International Methane Emissions Observatory, United Nations Environment Programme, Paris, France

[5]GHGSat Inc., Montreal, Canada

[6]Kayrros, Paris, France

*To whom correspondence should be addressed; E-mail: lguanter@fis.upv.es

List of Tables

S1 Summary of the emission rates derived from the high-resolution satellite observations passing the quality screening process 5

S2 Summary of the emission rates derived from the TROPOMI satellite observations passing the quality screening process 6

List of Figures

S1 Methane column concentration maps for the first observations of the Karaturun 2023 leak by Sentinel-5P/TROPOMI 7

S2 Time series of flux rate estimates obtained from the different satellites used in this work 8

S3 Comparison of the fire intensity at the Karaturun 2023 blowout site with that of other gas flaring events 9

S4 Empirical $U_{\mathrm{eff}} - U_{10}$ models for IME-based flux rate estimates from EnMAP, PRISMA and EMIT ΔXCH_4 retrievals 10

S5 Verification of ΔXCH_4 retrievals and flux rate estimates from hyperspectral data with end-to-end simulations 11

S6 Assessment of the potential distortion of ΔXCH_4 retrievals by water vapour and smoke 12

S7 Quantification of the total amount of methane released by the leak 13

Text S1. Quantification of methane plumes with TROPOMI

With daily global coverage, TROPOMI, onboard Sentinel-5P, enables global mapping of methane concentrations at 5.5×7 km^2 resolution using the shortwave infrared (SWIR) spectrum at $2.3\ \mu$m. For this analysis, we use version 02.05.00 of the TROPOMI-CH_4 operational product corrected for stripes[1] with a custom quality filter (qa value ≥ 0.4, SWIR aerosol optical thickness < 0.1, SWIR surface albedo > 0.05, surface classification $\neq 3$, and SWIR cloud fraction < 0.015).

Methane concentrations are simulated using the Weather Research and Forecast (WRF) version 4.1[2] around the blowout location at a 3×3 km^2 resolution for an area of 800×800 km^2 from June 2023 to December 2023. We perform simulations with both 6-hourly National Centre for Environmental Prediction (NCEP)[3] and hourly ERA5[4] meteorological fields. The 6-hourly Copernicus Atmosphere Monitoring Service (CAMS) atmospheric composition forecast data[5] is used to provide the initial and boundary conditions. To infer emissions, the Bayesian cost function J is minimized to optimize the state vector $\hat{\mathbf{x}}$[6]:

$$\hat{\mathbf{x}} = \mathbf{x}_A + \mathbf{S}_A \mathbf{K}^T (\mathbf{K}\mathbf{S}_A\mathbf{K}^T + \mathbf{S}_0^{-1}(\mathbf{y} - \mathbf{K}\mathbf{x}_A)) \quad (1)$$

where $\mathbf{x}_A$ is the prior state vector, considered 30 t/hr, $\mathbf{S}_A$ is the prior error covariance matrix assuming 10% uncertainty for the CAMS boundary conditions and 100% uncertainty for the blowout emissions, $\mathbf{K}$ is the Jacobian matrix, and $\mathbf{y}$ is the observational vector containing TROPOMI observations. The model output is resampled to match the TROPOMI pixel spatial footprint using TROPOMI averaging kernels. The observations and model are then aggregated to $0.2^\circ \times 0.2^\circ$ grids to negate model errors. $\mathbf{S}_0$, the observational error covariance matrix, is constructed as a diagonal matrix using the standard deviation of the difference between the prior modeled concentrations and TROPOMI observations.

To obtain a simulated plume that best matches the TROPOMI observed plume, we perform an ensemble of WRF simulations using: meteorological fields from either NCEP or ERA5, using four different planetary boundary layer physics options, and sampling the WRF outputs at the TROPOMI overpass time as well as up to 3 hours before and after the overpass time. Preliminary inversions are performed daily using the 56 simulated plumes, and the plumes with the lowest posterior observation cost function are selected. For the final inversion, we optimize the CAMS boundary conditions and the blowout emissions for each day. We only report quantifications for days with clear plumes, no potentially interfering downwind coastal artifacts, and good matches with simulated plumes based on visual inspection. We find that for all reported daily plume quantifications, the averaging kernel value for the blowout is above 0.5, showing the prior value has no significant impact on the estimated emissions. For estimating the uncertainty associated with the quantified emissions, an ensemble of inversions is computed by varying inputs and the assumptions used for the inversion[7]. This includes: increasing and decreasing the prior emissions for the blowout by a factor of 50%; using model outputs sampled every one hour before and after the overpass hour; using the second best plume match based on observation cost; performing the inversions using different aggregation resolutions $(0.15^{\circ}, 0.25^{\circ})$; using TROPOMI data with highest quality flag of 1 (qa value $= 1$); using TROPOMI data without filtering for albedo; and following the central limit theorem instead of using mean observational error when aggregating observations, giving us a total of 1728 ensemble members for each day.

	Sensor	Acquisition date	Wind (m/s)	Q (t/h)	Q_err (t/h)
1	Sentinel-2	09/06/2023	3.0	63.3	42.0
2	Landsat 8-9	30/06/2023	2.9	42.9	14.6
3	PRISMA	11/07/2023	8.6	41.9	20.9
4	PRISMA	17/07/2023	7.3	38.0	18.2
5	GHGSAT	22/07/2023	4.6	49.3	16.8
6	GHGSAT	23/07/2023	1.5	21.2	11.4
7	PRISMA	23/07/2023	2.5	18.7	6.7
8	Landsat 8-9	01/08/2023	5.8	47.0	19.1
9	PRISMA	03/08/2023	8.9	28.5	14.1
10	GHGSAT	08/08/2023	4.5	35.8	12.5
11	EMIT	10/08/2023	5.6	21.1	9.4
12	GHGSAT	11/08/2023	2.8	39.1	17.2
13	GHGSAT	11/08/2023	5.6	24.9	7.5
14	GHGSAT	12/08/2023	5.1	43.2	13.8
15	EMIT	14/08/2023	5.3	35.6	15.7
16	GHGSAT	15/08/2023	2.8	27.7	12.2
17	Landsat 8-9	17/08/2023	3.9	41.4	15.4
18	GHGSAT	30/08/2023	6.3	30.2	8.5
19	PRISMA	01/09/2023	3.9	28.9	12.0
20	GHGSAT	04/09/2023	5.6	29.6	8.9
21	PRISMA	07/09/2023	5.7	37.8	17.3
22	PRISMA	19/09/2023	4.0	22.7	9.5
23	ENMAP	23/09/2023	6.9	32.4	15.4
24	Landsat 8-9	26/09/2023	4.9	23.8	9.3
25	ENMAP	27/09/2023	4.7	15.3	6.7
26	GHGSAT	01/10/2023	2.6	13.9	6.1
27	ENMAP	08/10/2023	8.5	14.2	7.0
28	ENMAP	27/10/2023	4.8	27.9	12.2
29	ENMAP	04/11/2023	1.9	9.0	2.9
30	ENMAP	08/11/2023	8.1	26.1	12.8
31	GHGSAT	04/12/2023	4.5	3.6	1.3
32	GHGSAT	09/12/2023	9.7	3.9	0.9
33	GHGSAT	25/12/2023	8.2	11.8	2.7

Table S1: Summary of the emission rates derived from the high-resolution satellite observations passing the quality screening process. This quality screening has removed the observations with cloud contamination, retrieval artifacts and plumes for which a substantial part of the tail lied outside the imaged area. Q refers to the flux rate estimated for each plume, and Q_err to the associated 1-σ uncertainty.

	Sensor	Acquisition date	Q (t/h)	Q_err (t/h)
1	TROPOMI	23/06/2023	40.0	17.3
2	TROPOMI	26/06/2023	52.0	16.3
3	TROPOMI	06/07/2023	31.5	18.4
4	TROPOMI	11/07/2023	53.2	29.9
5	TROPOMI	12/07/2023	32.9	14.3
6	TROPOMI	07/08/2023	27.4	12.6
7	TROPOMI	08/08/2023	29.5	12.6
8	TROPOMI	09/08/2023	47.0	23.1
9	TROPOMI	21/08/2023	43.2	20.8
10	TROPOMI	24/08/2023	32.9	17.1
11	TROPOMI	31/08/2023	51.0	31.3
12	TROPOMI	01/09/2023	42.4	29.7
13	TROPOMI	02/09/2023	45.6	21.5
14	TROPOMI	03/09/2023	27.4	17.1
15	TROPOMI	21/09/2023	15.3	3.3

Table S2: Summary of the emission rates derived from the TROPOMI satellite observations passing the quality screening process. This quality screening has consisted in the selection of only clear plumes and of good matches with simulated plumes based on visual inspection. Q refers to the flux rate estimated for each plume, and Q_err to the associated 1-σ uncertainty.

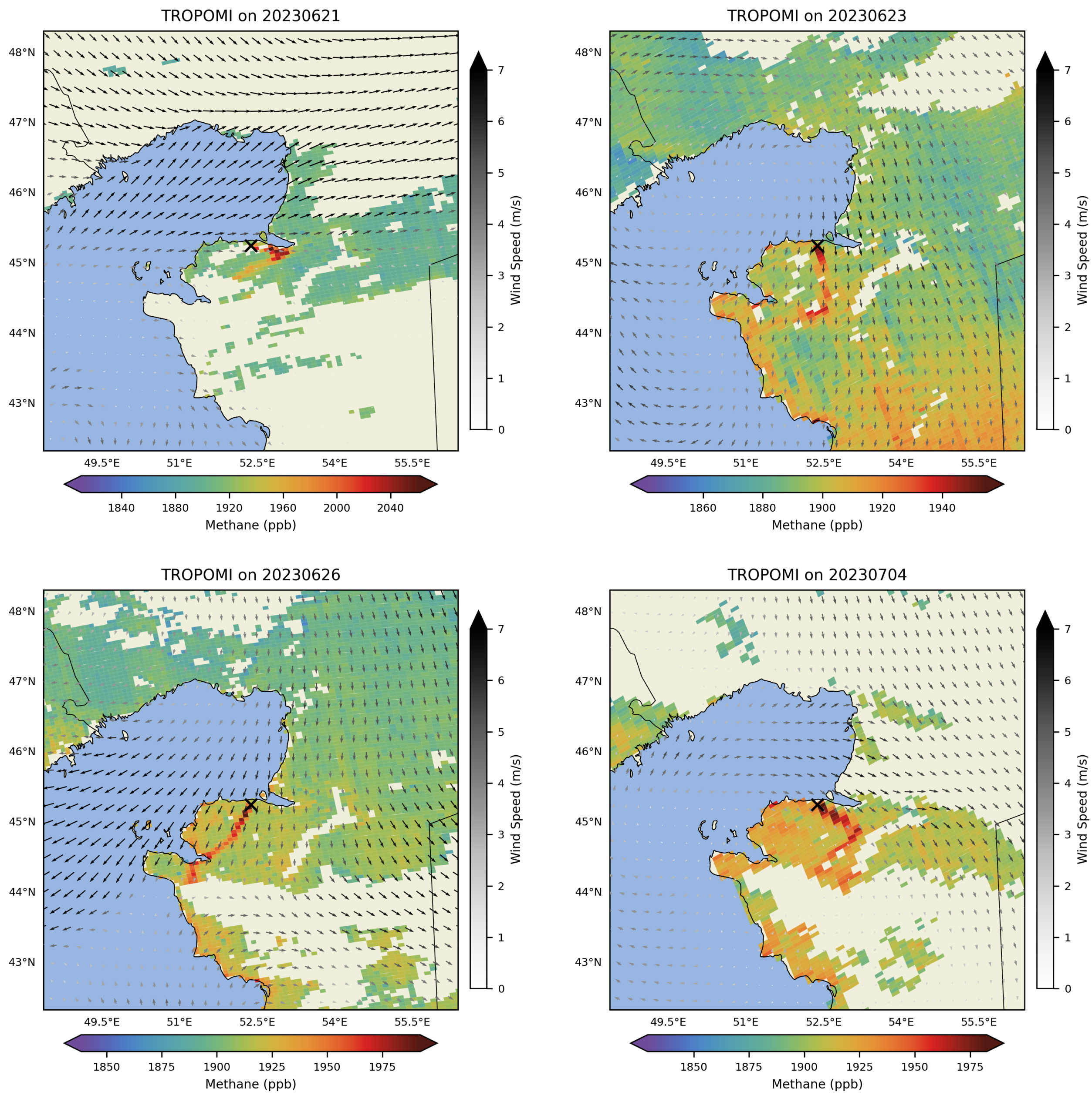

Figure S1: Methane column concentration maps for the first observations of the Karaturun 2023 leak by Sentinel-5P/TROPOMI. Data are from the TROPOMI-CH_4 operational product (02.05.00 version). The color scale indicates the total methane column concentration estimated from TROPOMI (as opposed to the concentration enhancement derived from the high resolution data). Arrows indicate wind intensity and direction. TROPOMI data on 21 June and 4 July were not used to quantify emissions as we could not obtain a good match with a modeled plume.

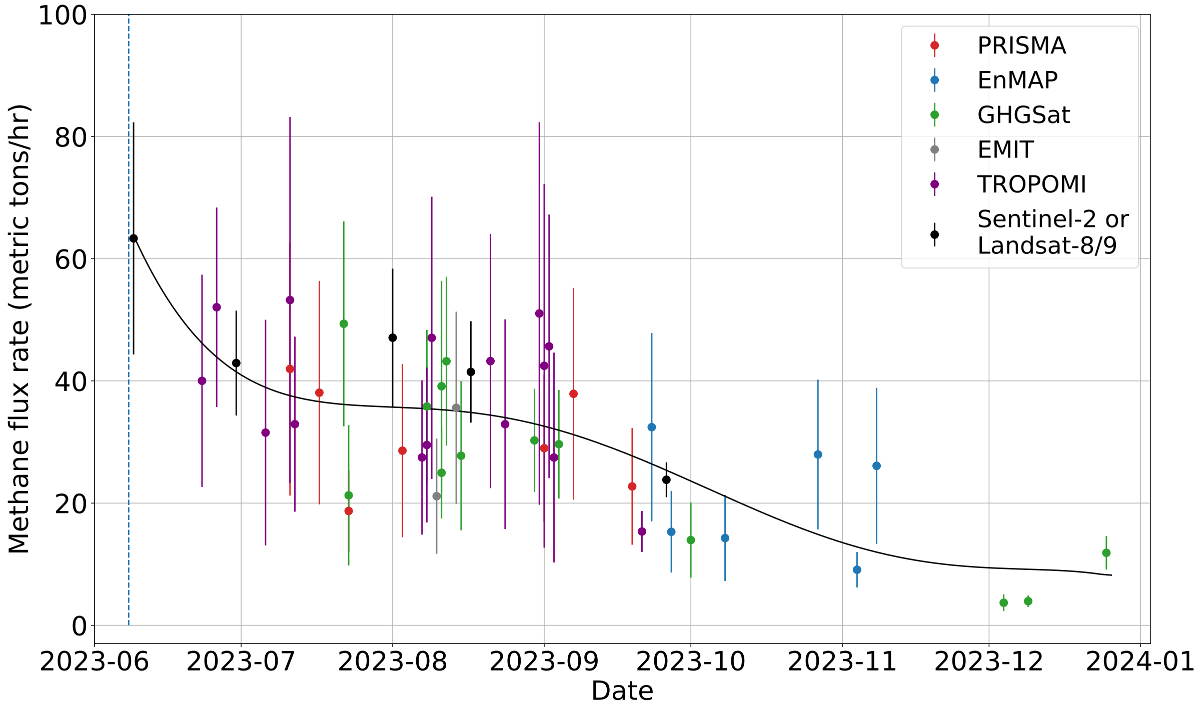

Figure S2: Time series of flux rate estimates obtained from the different satellites used in this work. The points represent the flux rate estimates for the 48 plumes retained for quantification after quality screening. This figure offers a more clear representation of the data derived from each satellite as compared with Fig. 3a of the Main Text.

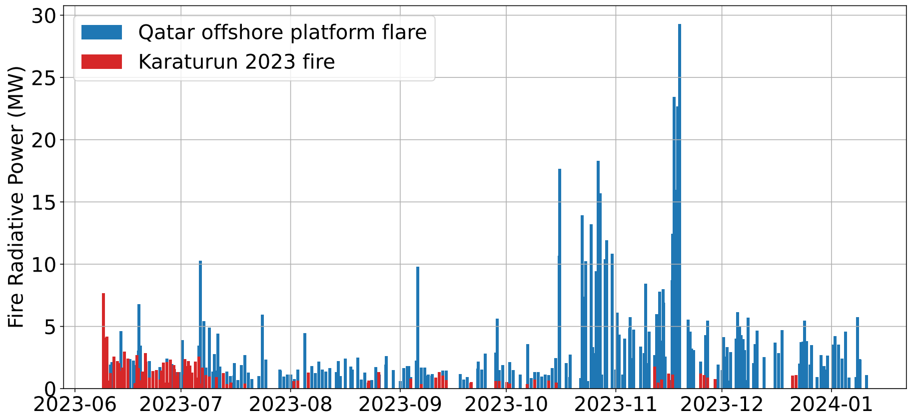

(a)

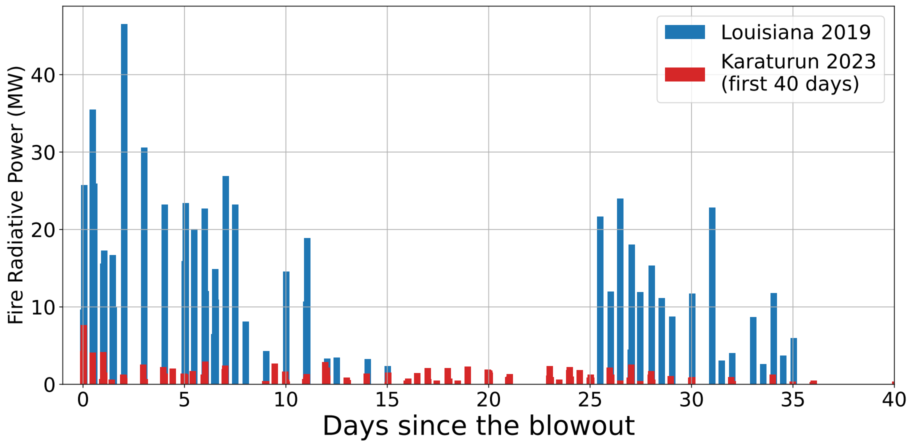

(b)

Figure S3: Comparison of the fire intensity at the Karaturun 2023 blowout site with that of other gas flaring events. (a) Regular flare in an offshore platform in Qatar (26.59°N, 52.00°E). (b) Fire intensity during the Louisiana 2019 event (Maasakkers et al., 2022), where gas burned first at the wellheads for two weeks, and then at a flare pit for 10 days, with a 10-day period in between during which the gas was vented. In both cases, fire intensity is proxied by the fire radiative power variable provided in the VIIRS Fire Information for Resource Management System (FIRMS) product.

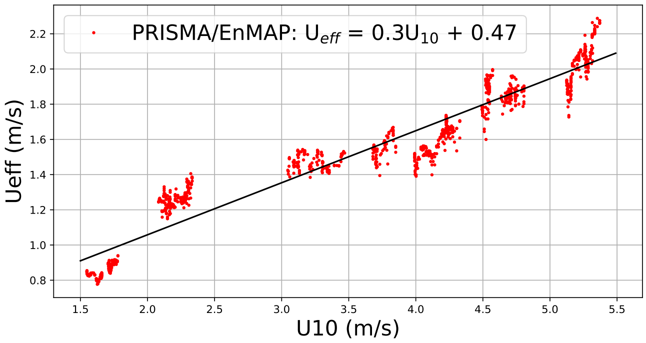

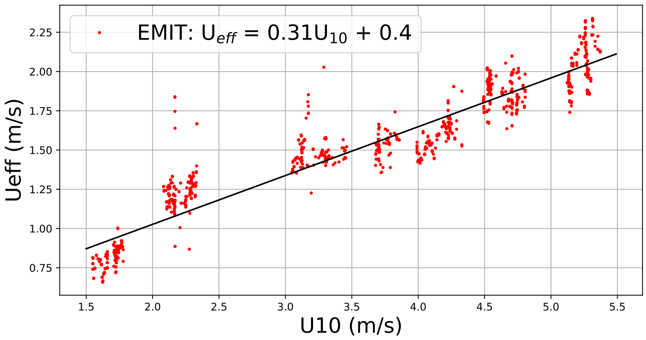

Figure S4: Empirical $U_{\mathrm{eff}} - U_{10}$ models for IME-based flux rate estimates from EnMAP, PRISMA and EMIT ΔXCH_4 retrievals. The linear models have been generated using a database of plumes simulated with a WRF-LES modeling approach. The plume simulations cover the flux rate range of 10–90 t/h, and are done for the ΔXCH_4 retrieval noise found in the Karaturun East site for those missions. Separate models have been generated for EnMAP-PRISMA and EMIT because of the different spatial sampling (30 m for EnMAP-PRISMA and 60 m for EMIT). Retrieval precision is assumed to be similar for EnMAP and PRISMA.

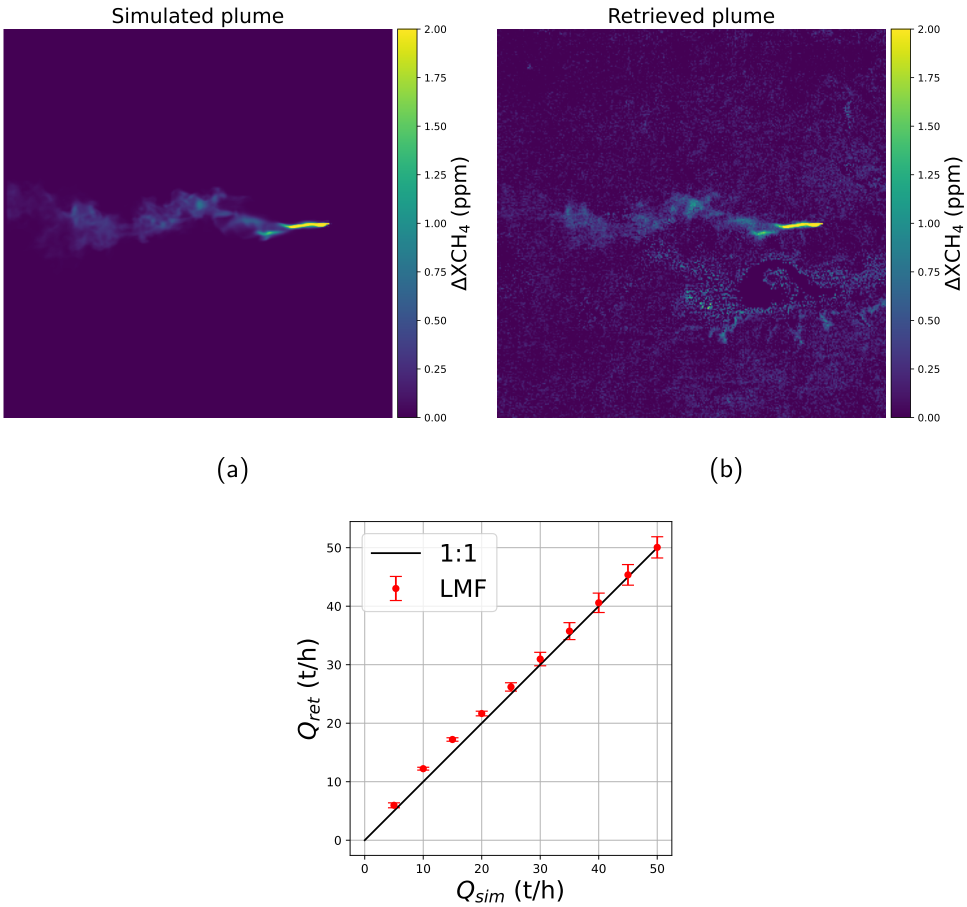

(a) (b) (c)

Figure S5: Verification of ΔXCH_4 retrievals and flux rate estimates from hyperspectral data with end-to-end simulations. (a), Simulated methane plume (25 t/h) added to a real PRISMA radiance dataset. (b), Methane plume retrieved from the processing of the resulting PRISMA radiance dataset using the ΔXCH_4 retrieval scheme implemented for this study. (c), Comparison of the input and estimated flux rates (Q_{sim} and Q_{ret}, respectively) from the entire end-to-end simulation process.

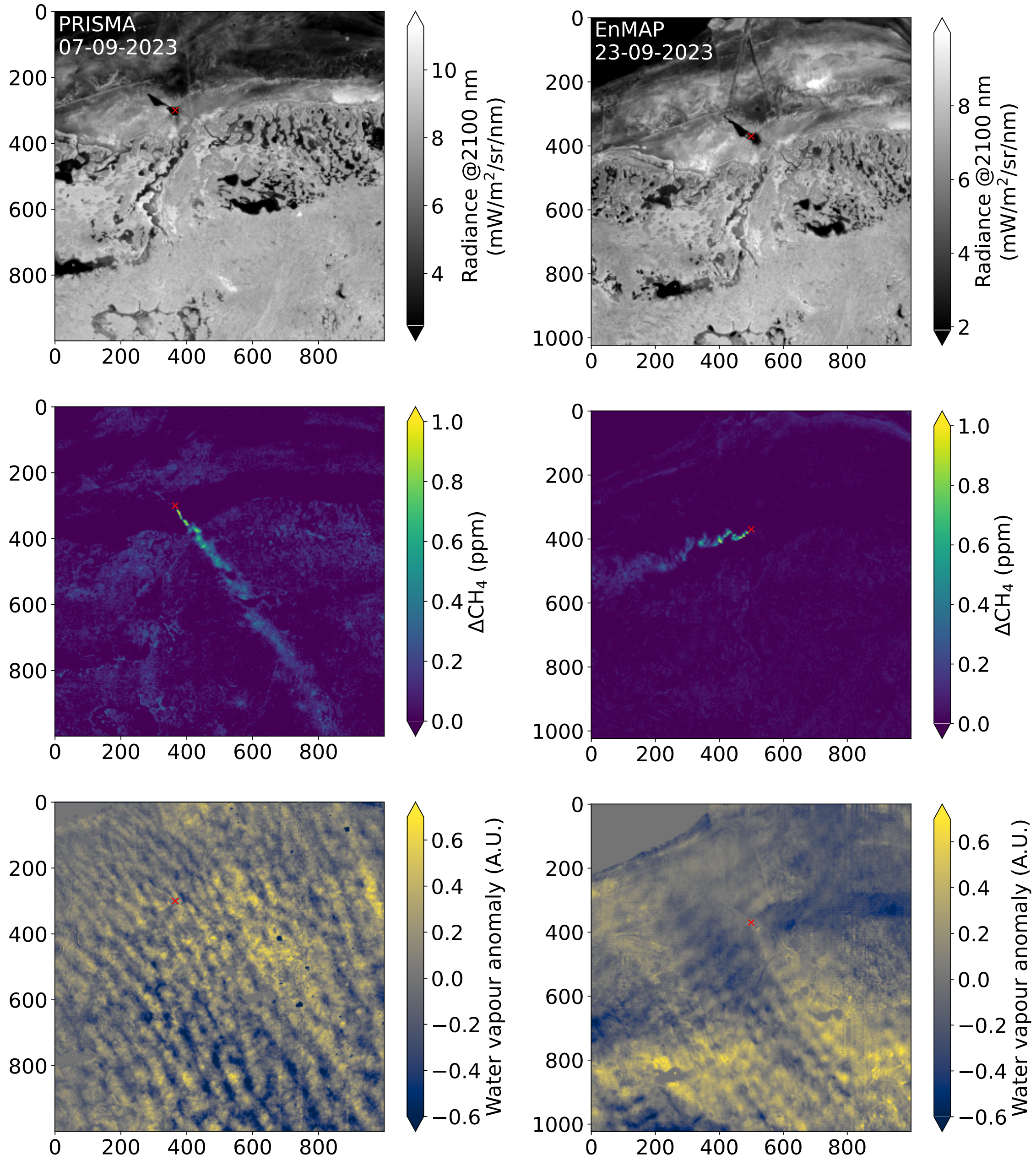

Figure S6: Assessment of the potential distortion of ΔXCH_4 retrievals by water vapour and smoke. Maps of at-sensor radiance at 2100 nm (top row), ΔXCH_4 (center row), and water vapour concentration anomaly (bottom row) derived from a PRISMA acquisition from 7 September 2023 (left column), and an EnMAP acquisition from 23 September 2023 (right column). No water vapour plume superposed to the methane plume can be observed from the comparison of ΔXCH_4 and water vapour anomaly maps. Also, no smoke plume can be observed in the 2100 nm radiance maps, which suggests that, in this particular event, smoke has a negligible optical activity on the shortwave infrared window from which ΔXCH_4 maps are retrieved.

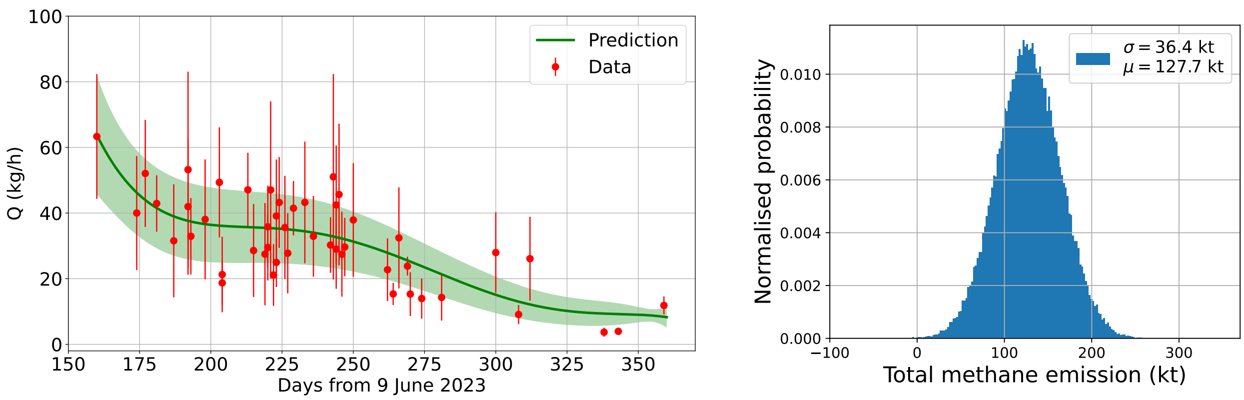

(a) All 48 high-quality plumes used for the total emission quantification (see Fig. 3a and Fig. S2)

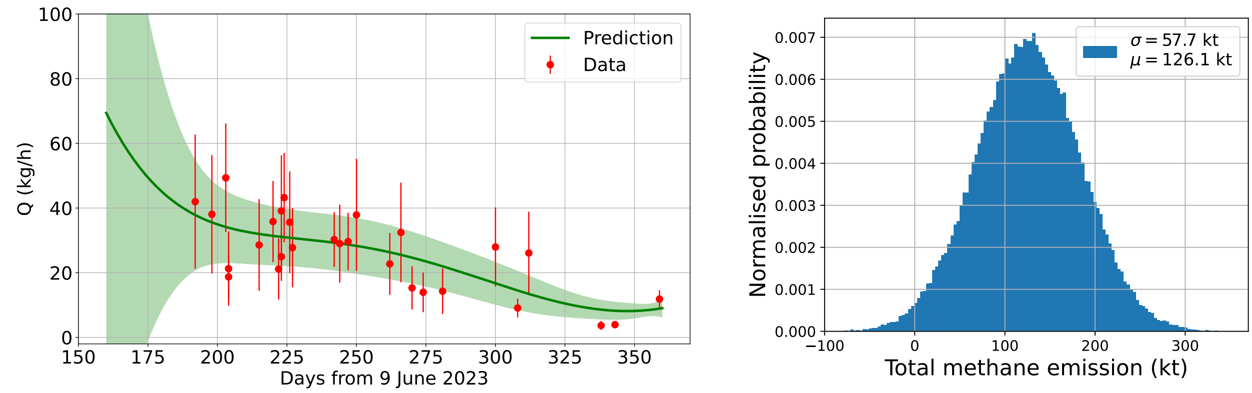

(b) Hyperspectral-only plume detections (PRISMA, EnMAP, EMIT, GHGSat)

Figure S7: Quantification of the total amount of methane released by the leak. Top row, results from the dataset consisting of the 48 high quality plumes (including TROPOMI as well as hyperspectral and multispectral high-resolution observations) used in this study for the quantification of the leak in this study. Bottom row, results from an alternative hyperspectral-only configuration. The time series on the left hand side depict a polynomial fit of the satellite-based flux rate estimates (Q) selected after quality screening. The fitted model is integrated to obtain an estimate of the total leak. The shaded green area corresponds to the uncertainty (k=1) of the flux rate fitting. The probability distribution functions on the right hand side show the result of propagating the temporal flux rate together with the uncertainty using multivariate Monte Carlo simulations. An error correlation of 0.5 is assumed for the individual satellite observations. The comparison between the top and bottom row illustrates the fact that the extra observations from TROPOMI and the multispectral missions contribute to decrease the uncertainty range but have a very low impact on the total emission estimate.

References

1. Borsdorff, T. *et al.* Measuring carbon monoxide with tropomi: First results and a comparison with ecmwf-ifs analysis data. *Geophysical Research Letters* **45**, 2826–2832 (2018). URL https://agupubs.onlinelibrary.wiley.com/doi/abs/10.1002/2018GL077045. https://agupubs.onlinelibrary.wiley.com/doi/pdf/10.1002/2018GL077045.

2. Powers, J. G. *et al.* The weather research and forecasting model: Overview, system efforts, and future directions. *Bulletin of the American Meteorological Society* **98**, 1717 – 1737 (2017). URL https://journals.ametsoc.org/view/journals/bams/98/8/bams-d-15-00308.1.xml.

3. National Centers for Environmental Prediction, National Weather Service, NOAA, U.S. Department of Commerce. Ncep fnl operational model global tropospheric analyses, continuing from july 1999 (2000). URL https://doi.org/10.5065/D6M043C6.

4. Hersbach, H. *et al.* The era5 global reanalysis. *Quarterly Journal of the Royal Meteorological Society* **146**, 1999–2049 (2020). URL https://rmets.onlinelibrary.wiley.com/doi/abs/10.1002/qj.3803. https://rmets.onlinelibrary.wiley.com/doi/pdf/10.1002/qj.3803.

5. N, K. & P, B. Evaluation of copernicus atmosphere monitoring service methane products (2018).

6. Jacob, D. J. *et al.* Satellite observations of atmospheric methane and their value for quantifying methane emissions. *Atmospheric Chemistry and Physics* **16**, 14371–14396 (2016). URL https://acp.copernicus.org/articles/16/14371/2016/.

7. Maasakkers, J. D. *et al.* Using satellites to uncover large methane emissions from landfills. *Science Advances* **8**, eabn9683 (2022). URL https://www.science.org/doi/abs/10.1126/sciadv.abn9683. https://www.science.org/doi/pdf/10.1126/sciadv.abn9683.